Using Dielectric Orthotropy as an Indicator of Internal Decay of Wood Members

C. Adam Senalik
USDA, Forest Service, Forest Products Laboratory, Madison, WI, USA, christopher.a.senalik@usda.gov

Benjamin Farber
Mississippi State Univ., College of Forest Resources, Dept. of Sustainable Bioproducts, Starkville, MS, USA, bf720@msstate.edu

James P. Wacker
USDA, Forest Service, Forest Products Laboratory, Madison, WI, USA, james.p.wacker@usda.gov

Xiping Wang
USDA, Forest Service, Forest Products Laboratory, Madison, WI, USA, xiping.wang@usda.gov

Abstract

Several material properties of wood are directionally dependent. Mechanical properties such as tension, compression, and bending strength vary greatly for the same piece of wood when tested parallel to the grain (longitudinally), perpendicular to the grain and parallel to the annual rings (tangentially), or perpendicular to both the grain and rings (radially). For this reason, wood is often considered to be a cylindrically orthotropic anisotropic material. The orthotropy extends to dielectric properties of wood. However, in the presence of internal decay, the directional dependency of the dielectric qualities diminishes. By identifying and measuring the loss of directional dependency, the presence and extent of internal decay is evaluated. Ground penetrating radar (GPR) is used as the inspection tool. A bowtie, bistatic, dipole antenna with a center frequency of 2 GHz is used for measurement. The specimens are wood members of sizes typically used in bridge construction. The GPR technique has several advantages over existing non-destructive testing (NDT) techniques: it requires access to only one side of the specimen, no special methods are needed to couple the sensor to the specimen, and it uses a commercially available tool already accepted within the NDT industry. This study is part of a larger study to develop improved NDT tools for timber bridge inspection.

Keywords: Ground penetrating radar, GPR, glulam, bridge timbers

Introduction

Since the turn of the century, interest in ground penetrating radar (GPR) as an inspection tool for wooden structures has increased (Rodrigues, B. et al. 2021). GPR allows rapid scanning of the target specimen, detects several types of subsurface features, detects the presence of moisture, and does not require direct contact between the sensor and target (Mai et al 2015a, Cassidy 2009, Müller 2002, Müller 2003, Rodríguez-Abad 2008, Hans et al. 2015a, Hans et al. 2015b). Alongside the advantages are complicating factors. Wood is a dispersive material, so the radar wave frequency affects how the wave travels through the target specimen. In addition, the transmitting wave may be affected by any combination of temperature, moisture content, geometry of the specimen and/or internal features, and density (Mai et al 2015, Hans et al. 2015a, Hans et al. 2015b, Torgovnikov 1993). When the impact of the complicating factors is understood, GPR becomes a powerful inspection tool. The United States Department of Agriculture (USDA), Forest Service (FS), Forest Products Laboratory (FPL), in conjunction with the U.S. Federal Highway Administration (FHWA) recently initiated a multiphase study to develop GPR into a viable inspection tool for wood structures (Senalik et al. 2016). The goal of the overall study is to develop improved NDT tool for timber bridge inspection.

Background

The ability of GPR to locate fungal decay is examined here. Normally fungal decay is collocated with pockets of moisture within the wood beam. In this study, the specimens were conditioned to 12% moisture content (MC) to remove the pockets of internal moisture to quantify the sensitivity of GPR to fungal decay alone. The method used to locate the decay monitors change in dielectric constant (DC) parallel to the grain ($DC_{//}$) relative to the DC perpendicular to the grain ($DC_{\perp}$). DC is the capacitance of a material relative to the capacitance of a vacuum. It is expressed as a unitless ratio with a range of values of 1 for air to over 80 for pure water. DC is affected by temperature, relative humidity, and wave frequency. The specimens in this study are constructed of Douglas-fir which has DC values around 2.3 parallel to the grain and 1.8 perpendicular to the grain at 22.8°C, 12% MC, and 2 GHz (Torgovnikov 1993, Wittkopf and MacDonald 1949, Mai 2015b, Rodríguez-Abad 2010). As wood decays, $DC_{//}$ decrease more quickly than $DC_{\perp}$. As a result, by monitoring the DC change relative to each direction, internal decay can be identified.

Materials and Methods

The specimens in this study are Douglas-fir (*Pseudotsuga menziesii (Mirb)Franco*) glued-laminated beams with rectangular cross sections typical of those used in bridge construction. The specimens are inoculated with brown rot fungus known to be aggressive against the Douglas-fir species (*Fomitopsis pinicola (Sw.) P.Karst. (1881)*) and exposed to field conditions for 46 months in the Harrison Experimental Forest in Mississippi, USA, which is approximately 40-km north of the Gulf of Mexico. The conditions at the exposure site promotes fungal growth. The treatment of the specimens is extensively described in (Senalik et al. 2016, Senalik et al. 2017). A diagram of a typical specimen is shown in Figure 1a. The four fungal cavities are shown: one in each end and two on the top face near the ends. Scan direction is relative to the metal identification (ID) tag on each specimen.

The specimens include two glulam beams: a six-layer glulam beam with cross-sectional dimensions of 13.0-cm × 22.7-cm and a five-layer glulam beam with dimensions of 13.0-cm × 17.8-cm. Both beams are 81.3-cm in length. After field exposure, the specimens are returned to FPL and inspected using X-ray computer tomography (CT) to identify areas of decay (Senalik et al. 2019, Bucur 2003). Hereafter, the six-layer glulam will be referred to as specimen A and the five-layer is specimen B. After CT, the specimens are stored in an environmentally controlled room (22.8°C and 50% relative humidity (RH)) for 28 months to reach an equilibrium moisture content (EMC) of 12%. At that time, the specimens are scanned using GPR with a center frequency of 2-GHz. The GPR and antenna which emits the radar waves are a commercially available unit from Geophysical Survey Systems, Inc. from Nashua, NH (GSSI). The unit is a GSSI SIR® 4000 GPR data acquisition system and a 2-GHz MHz dipole bowtie antenna (DBA) (GSSI 2014). A typical GPR output scan, a radargram, is shown in Figure 1b. The dark band at approximately 350 ns/$DC^{1/2}$ represents the far edge of the specimen. Note the distortion to the shape of the curve near the ends of the specimen.

Each face of each specimen is scanned with the GPR DBA oriented such that the electromagnetic field generated is parallel to the grain (this orientation is designated $ef_{//}$ for brevity; $ef_{\perp}$ for perpendicular). It is from these scans that $DC_{//}$ is determined. An aluminum plate is placed on the side of the specimen opposite of the antenna to create a strongly reflective boundary which facilitates the identification of the far edge of the specimen in the GPR output. The scanning regime is shown in Figure 2. On the top face, the edge of the palm antenna is aligned with the edge of beam and scanned towards the ID tag. This produces a scan through the depth of the specimen (top to bottom). For the second scan, the DBA uses the same scan line, but scans away from the ID tag. Due to the design of the DBA, approximately 2-in of the end of the specimen where the scan begins are missed. The scan away from the metal ID tag provides the information on the lost 2-in. The data from both scans are merged to provide a single output for the entire length of the specimen. Since decay often enters wood at the cut ends, it is important that the overall scan contain as much information about the end of the specimens as possible. The third and fourth scans are in the same directions as the first and second, but the palm antenna is aligned with the opposite edge of the specimen.

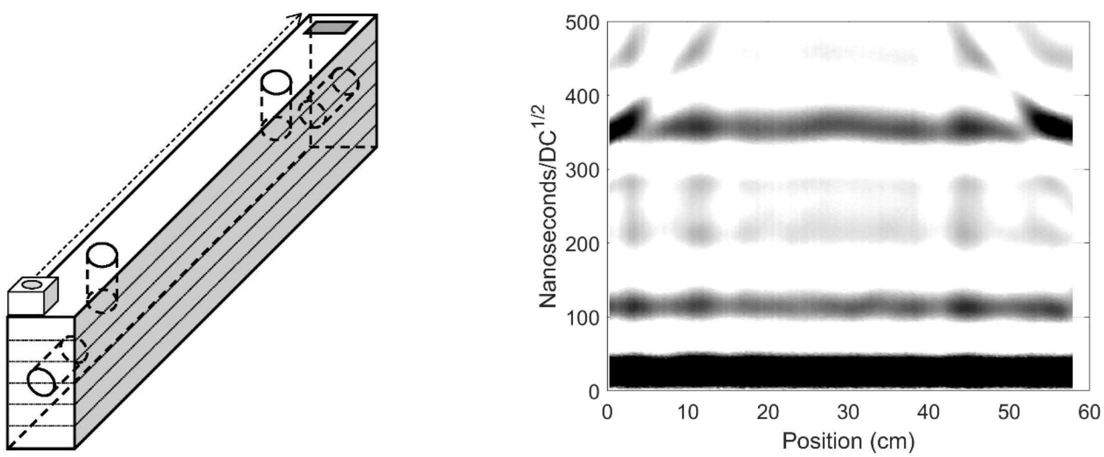

a. b.

Figure 1 - Diagram of typical specimen and a typical radargram. a) Diagram of typical 6-layer glulam beam specimen. The white box with the gray circle on top represents the GPR antenna. The arrow represents the direction the antenna is moved during a GPR scan. b) Typical radargram from a longitudinal GPR scan. The prominent black line at approximately 350 ns/DC$^{1/2}$ is the bottom edge of the specimen.

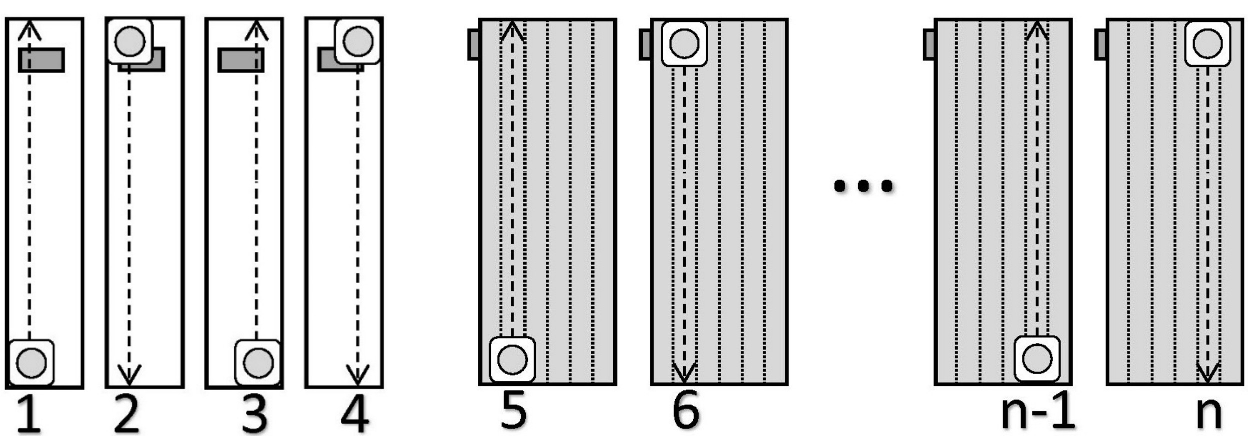

a. b.

Figure 2 - GPR scanning regime of specimens. The dark rectangle at the top of the specimens represents the metal identification tag. The white box with the gray circle represents the GPR antenna. The arrow represents the direction of motion of the antenna during scanning a) Scanning of top and bottom surfaces. b) Scanning of side surfaces. Only the inner layers are scanned. The top and bottom layers are not scanned as the antenna will overhang the edge of the specimen.

On the sides of the specimen, the scan lines are along the centerline of each of the interior lamina. The top and bottom lamina are excluded from scanning as the antenna will overhang off the edge of the specimen causing the output to be some mixture of wood and air. The fifth specimen scan is the second lamina from the top in the direction towards the ID tag; the sixth is the same scan line away from the ID tag. Scans along the side are across the width of the specimen. The process is repeated for each of the interior lamina and for the same lamina with the antenna positioned on the opposite side of the specimen. GPR scans of the bottom of the specimen mirror those taken on the top. The entire scanning process is then repeated with the GPR DBA oriented such that $ef_{\perp}$ is generated and $DC_{\perp}$ is determined.

Decay detection makes use of the difference in DC parallel and perpendicular to the wood grain. Early in the study, there was an examination of the proportional reduction in DC parallel to the grain relative to the proportional change in DC perpendicular to the grain as a method of identifying decay regions. Unfortunately, the proportional change in $DC_{//}$ too close to that of $DC_{\perp}$ to make accurate predictions. At that point, the method was altered to look at the absolute change in $DC_{//}$ relative to the absolute change in $DC_{\perp}$. Since $DC_{//}$ is larger than $DC_{\perp}$ and the proportional change in DC for both directions was found to be similar, the absolute reduction is $DC_{//}$ must be greater than that of $DC_{\perp}$. At this point, a threshold differentiating sound and decayed wood is needed. The threshold is developed from control specimens. The decision to develop the threshold from control specimens rather than initial GPR of the specimens prior to field exposure is made as a consideration of the information that will be available to inspectors in the field. It is unlikely they will have early time GPR information of wood bridge timbers, and would rely upon information gleams from similar beams that have not been field exposed.

Threshold Development

Two five-layer glulam beams with the same cross-sectional dimensions as specimen B were used as control specimens. The control specimens were cut from the same beams that were used to make the five-lamina field exposed specimens. The control specimens are designated as C1 and C2. From the control specimens, two analysis methods were developed: compensation for geometric distortion of the GPR output caused by proximity to the end of the beam, and threshold value contour identifying likely areas of decay.

As the DBA nears the end of the specimens, reflections from the wood air boundary at the end of the specimen cause distortion of the GPR output. This distortion is a function of the thickness of the specimen under the DBA and the distance between the DBA to the end of the specimen. To compensate for this distortion, a shape factor based upon distance from the edge of the specimen is determined. Shape factors are generated for scans through the depth and across the width for $ef_{//}$. For brevity, the process of developing the shape factor is shown only for scans across the width with $ef_{//}$. When the DBA is far from the end of the specimen, the reflection for the far edge of the specimen is mostly constant (Region 1 in Figure 3a). As the DBA approaches the end of the specimen, the data recorded by the GPR is a combination of the reflection from the far edge and the reflection from the end of the specimen (Region 2). As the DBA continues to approach the end of the specimen, the reflection from the end of the specimen becomes the dominant source of information in the output (Region 3). While the compensation cannot recover specimen condition information that is both near the end and near the far edge, it does lessen the influence of the boundary effects on the output.

In Figure 3a the end distortion is shown for several scans through the width of the control specimens. The Regions described above are identified. The first step in compensating for the end effect distortion is to normalize each scan by the respective mean value of Region 1 to yield a factional value for each data point as shown in Figure 3b. The fractional values (ordinate or y-values) are averaged for at each location (abscissa or x-values) to form a single curve as shown in Figure 3c. The values along the curve are the shape factor. Each point of the raw scan is divided by the fractional value of the shape factor to remove the end effect distortion. An example of the application of the shape factor curve is shown in Figure 3d and Figure 3e.

The next step is to develop a threshold criterion that differentiates between sound and decayed wood. After the shape factor is applied to the raw data, the region of the $DC_{//}$ curve with the lowest coefficient of variation across a window of 3.8-cm is located. The window length of 3.8-cm was chosen as it is the approximate width of the DBA. When the region is found, the mean of the region is subtracted from all points on the $DC_{//}$ curve. The same window is then applied to $DC_{\perp}$, and the mean of the values is subtracted from all points on the $DC_{\perp}$ curve. As a result, the two curves vary about the zero DC value, and any variation in the curves is due to variations in the wood or the presence of decay. The parallel and perpendicular curves that vary about the zero DC value are referred to as $DC^0_{//}$ and $DC^0_{\perp}$. An example is shown in Figure 4a and Figure 4b. The final step is to subtract the values of the $DC^0//$ curve from the $DC^0_{\perp}$ curve. The resulting difference curve is used to locate areas decayed wood. An example is shown in Figure 4c.

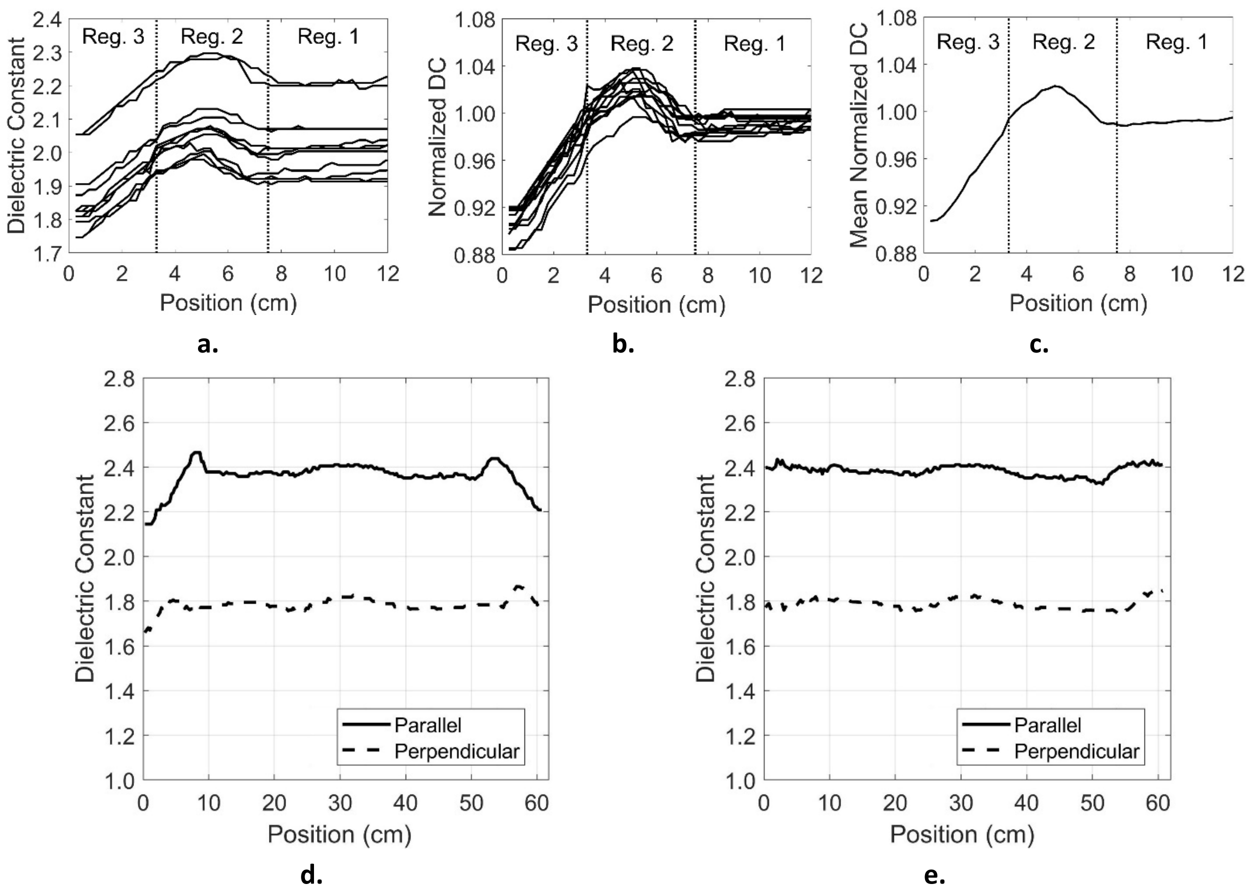

Figure 3 - Reducing end effect distortion with shape factor curve. a) Several scan outputs with end effect distortion. Region 1 is not affected by the end boundary. Region 2 is affected by both end boundary and the far edge. Region 3 is affected by the end boundary. b) Each scan is normalized by the mean value of Region 1. c) Normalized scans are averaged to yield the shape factor curve. d) A typical scan output with end effect distortion. e) The same scans when corrected by dividing the values by the shape factor curve values.

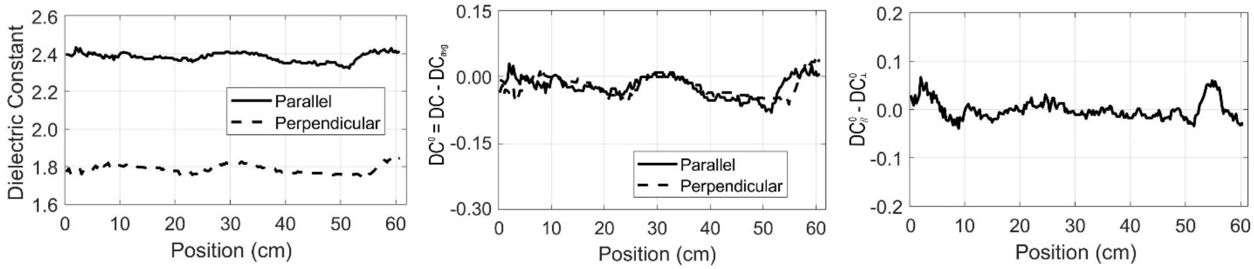

a. b. c.

Figure 4 - Calculating difference in DC parallel and perpendicular to grain. a) DC curves with end adjustment (same as Figure 3e) b) Curves adjusted to remove average DC value ($DC^0 = DC - DC_{avg}$) c) Difference between curves ($DC^0_{//} - DC^0_{\perp}$)

The threshold criterion is developed using all the DC difference curves from the control specimens. As shown in Figure 5a the values for all the curves are combined into a single data set. For any given point along the beam length, all the data from all the curves within ±1.9-cm of the given data point are combined into a single data set. The average and standard deviation of the data set are calculated. The threshold is set at the mean minus two standard deviations. This process is repeated for every point along the beam length to generate the threshold curve. The threshold line is shown as a white line in Figure 5a. Figure 5b is an overhead view of Figure 5a; the threshold curve is shown as a dashed black line. Values that fall below the threshold line indicate decayed wood.

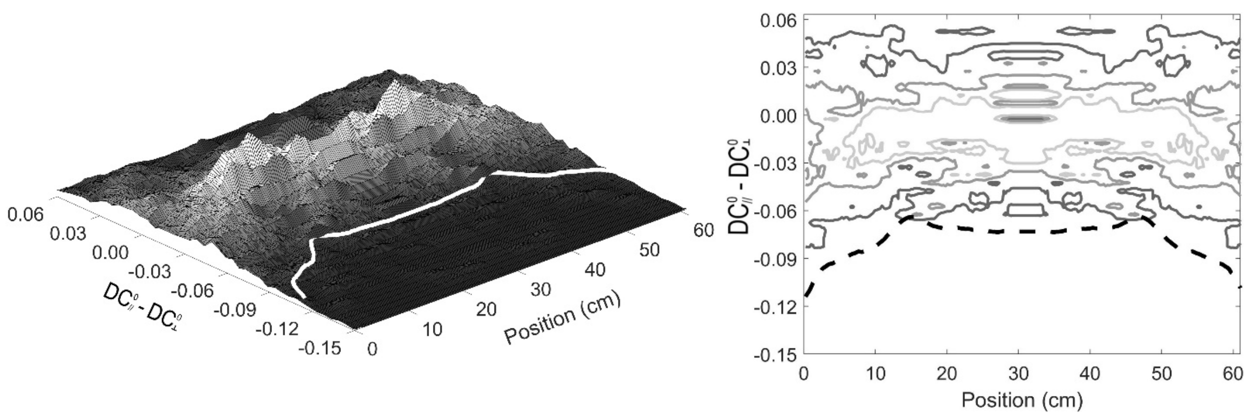

a. b.

Figure 5 - Development of the threshold curve identifying decayed wood using control specimens. a) A histogram plot by location along the control specimens. The white line is the threshold curve which is determined as two standard deviations below the mean DC for that location. b) A plan view of Figure 5a. The threshold curve is shown here as a black dashed line.

Results

Figure 6a and Figure 6b shows a scan of the A and B specimen, respectively, as well as the threshold curve for each. Based upon the threshold curve for specimen A, it would be predicted that decay would be found within the ranges of 0 to 26-cm and above 66-cm. It would be expected that the decay would be more severe in the 0 to 26-cm range than above 66-cm. Figure 7 and Figure 8 show the decay map developed for the A and B specimen, respectively, using the X-ray CT. The method of developing the decay map is described in (Senalik 2019). For the A specimen, there is considerable advanced decay from top to bottom of the specimen from 0 to 26-cm. Also, at 66-cm and above, there is advanced decay at the top and middle of the specimen, but the lower portion of the specimen appears to be sound.

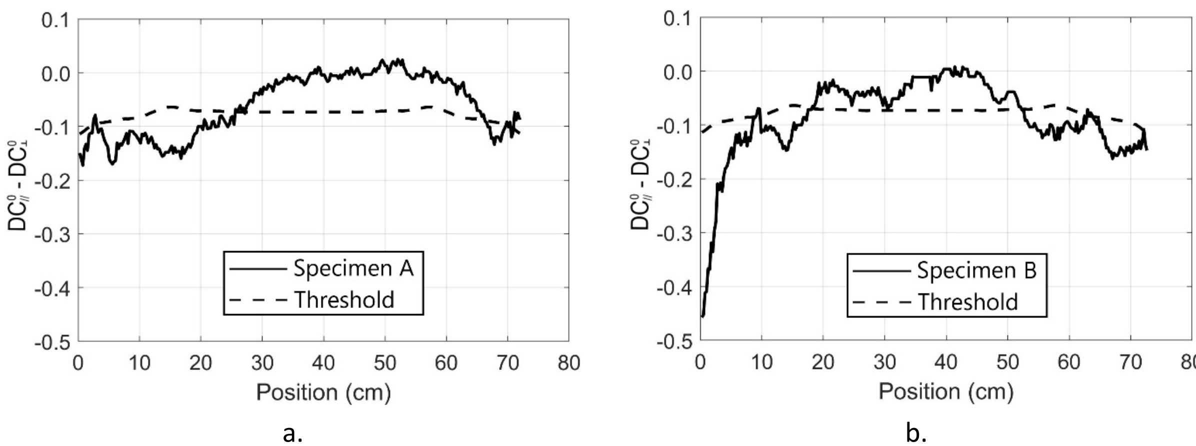

Figure 6 - DC difference plots for specimens A and B. a) The plot predicts decay from 0 to 26-cm and above 66-cm. b) The plot predicts decay below 18-cm and above 52-cm.

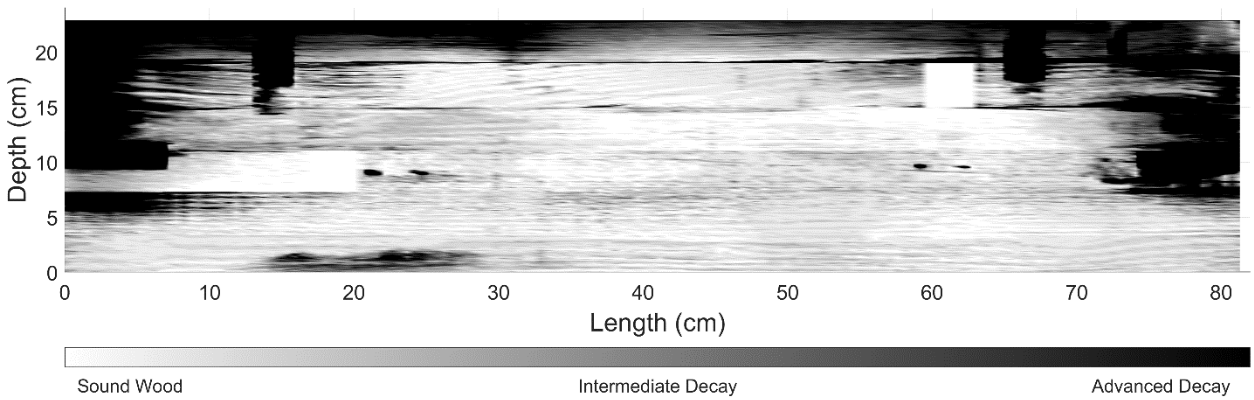

Figure 7 - Decay map of specimen A. In general, decay spreads out from the four fungal cavities and from the ends of the specimen. Advanced decay is present from top to bottom from 0 to 32-cm. There is advanced decay visible along the top surface. From 64 to 80-cm advanced decay is present in the top four lamina, but the bottom two lamina appear to be sound wood.

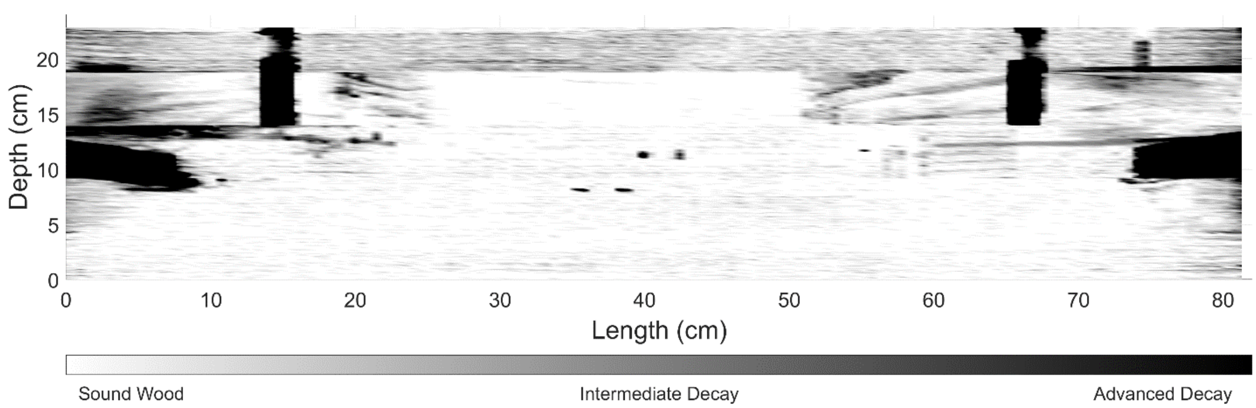

Figure 8 - Decay map of specimen B. In general, decay spreads out from the four fungal cavities and from the ends of the specimen. Advanced decay is present in the top three lamina from 0 to 23-cm. There is intermediate decay along some portions of the top lamina but it is only visible near the ends. There is a small region of advanced decay at 55-cm with larger areas at 67-cm and above.

Figure 6b shows a scan of the B specimen as well as the threshold curve. Based upon the threshold curve, it would be predicted that decay would be found within the ranges of 0 to 18-cm and above 52-cm. It would be expected that the decay would be more severe in the 0 to 5-cm range than any other region of specimen B. Figure 8 shows the decay map developed for the B specimen using the X-ray CT. From 0 to 23-cm, advanced decay is visible in the top three lamina with the highest concentration from 0 to 7-cm. There is intermediate decay along the top lamina, but it is only visible near the ends of the specimen. A small region of advanced decay is between 53 and 58-cm. Small regions of advanced decay are present between 65 and 80-cm.

Conclusions

For both specimens, A and B, there is good agreement between locations of interior decay and the difference in DC parallel versus perpendicular to the grain. As expected, wood decay decreases the DC of the wood and the DC parallel to the grain decreases quicker than DC perpendicular to grain in the presence of decay. A method is proposed for compensating for the distortion of the GPR signal near the end of the specimens using a shape factor. The shape factor method needs additional refinement to improve the performance for 6-lamina glulam. The coefficient of variation of the $DC_{//}$ values is used to identify the portion of the specimens that contain the least decayed wood. While COV results agree with X-ray CT scans, additional work is necessary to determine if this is the best method for identifying regions of sound wood. Finally, the DC difference values from control specimens are used to develop a threshold curve for decayed wood. The threshold of two standard deviations below the mean DC difference is used. Additional analysis may yield a better threshold estimate.

Acknowledgments

This study is part of the Research, Technology, and Education portion of the National Historic Covered Bridge Preservation (NHCBP) Program administered by the United States Department of Transportation, Federal Highway Administration. The NHCBP program includes preservation, rehabilitation, and restoration of covered bridges that are listed or are eligible for listing on the National Register of Historic places; research for better means of restoring and protecting these bridges; development of educational aids; and technology transfer to disseminate information on covered bridges to preserve the Nation's cultural heritage.

References

Bucur, V. 2003. Nondestructive characterization and imaging of wood. Berlin Heidelberg New York: Springer.

Cassidy, N.J. 2009. Electrical and Magnetic Properties of Rocks, Soils and Fluids. In Ground Penetrating Radar Theory and Applications; Elsevier: Amsterdam, The Netherlands; pp. 41–72.

Geophysical Survey Systems, Inc (2014) SIR 4000 manual. Geophysical Survey Systems, Inc., Nashua, NH. https://www.geophysical.com/wp-content/uploads/2017/10/GSSI-SIR4000-Manual.pdf .

Hans, G.; Redman, D.; Leblon, B.; Nader, J.; La Rocque, A. 2015a. Determination of log moisture content using early-time ground penetrating radar signal. Wood Mater. Sci. Eng. 2015, 10, 112–129.

Hans, G.; Redman, D.; Leblon, B.; Nader, J.; La Rocque, A. 2015b. Determination of log moisture content using ground penetrating radar (GPR). Part 1. Partial least squares (PLS) method. Holzforschung 2015, 69, 1117–1123.

Mai, T.C.; Razafindratsima, S.; Sbartaï, Z.M.; Demontoux, F.; Bos, F. 2015a. Non-destructive evaluation of moisture content of wood material at GPR frequency. Constr. Build. Mater. 77, 213–217.

Mai, T.C.; Sbartaï, Z.M.; Bos, F. 2015b. Non-destructive evaluation of wood moisture content using GPR technique—Effect of fiber direction and wood type. In Proceedings of the International Symposium Non-Destructive Testing in Civil Engineering (NDT-CE), Berlin, Germany, 15–17 September 2015.

Müller, W. 2002. Trial of ground penetrating radar to locate defects in timber bridge girders. In Proceedings of the Riding the Wave to Sustainability: IPWEAQ 2002 State Conference, Nossa Lakes, Queensland, Australia, 6–10 October 2002.

Müller, W. 2003. Timber girder inspection using ground penetrating radar. Insight Non Destr. Test. Cond. Monit. 2003, 45, 809–812, doi:10.1784/insi.45.12.809.52990.

Rodrigues, Brunela Pollastrelli; Senalik, Christopher Adam; Wu, Xi; Wacker, James. 2021. Use of Ground Penetrating Radar in the Evaluation of Wood Structures: A Review. Forests. 12(4): 492. https://doi.org/10.3390/f12040492.

Rodríguez-Abad, I.; Martínez Sala, R.; García-García, F.; Capuz Lladró, R.; Diez Barra, R. 2008. A non-destructive method for the evaluation of density and moisture content. In Proceedings of the 12th International Conference on Ground Penetrating Radar, Birmingham, UK, 16–19 June 2008.

Rodríguez-Abad, I.; Martínez-Sala, R.; García-García, F.; Capuz-Lladró, R. 2010. Non-destructive methodologies for the evaluation of moisture content in sawn timber structures: Ground penetrating radar and ultrasound techniques. Near Surf. Geophys. 2010, 8, 475–482, doi:10.3997/1873-0604.2010048.

Senalik, C.A.; Wacker, J.P.; Wang, X.; Jalinoos, F. 2016. Assessing the Ability of Ground Penetrating Radar to Detect Fungal Decay in Douglas-Fir Beams. In: 25th ASNT Research Symposium: Summaries and Abstracts. Paper presented at 25th Research Symposium, New Orleans (110-116). Columbus, OH: American Society for Non-destructive Testing, Inc. 7 p.

Senalik, C. Adam; Wacker, James P.; Wang, Xiping; Rodrigues, Brunella Pollastrelli; Jalinoos, Frank. 2017. Assessing ability of ground penetrating radar to detect internal moisture and fungal decay in Douglas-fir beams. In: Wang, X.; Senalik, C.A.; Ross, R.J., eds. Proceedings, 20th international non-destructive testing and evaluation of wood symposium. General Technical Report. FPL-GTR-249. Madison, WI: U.S. Department of Agriculture, Forest Service, Forest Products Laboratory: 286-300.

Senalik, Christopher Adam; Wacker, James; Wang, Xiping; Wu, Xi. 2019. Identifying incipient decay in Douglas-fir bridge components using x-ray computerized tomography. In: Wang, X.; Sauter, U.H.; Ross, R.J., eds. 2019. Proceedings: 21st International Nondestructive Testing and Evaluation of Wood Symposium. General Technical Report FPL-GTR-272. Madison, WI: U.S. Department of Agriculture, Forest Service, Forest Products Laboratory: 62-70.

Torgovnikov, G.I. 1993. Dielectric Properties of Wood and Wood-Based Materials; Springer-Verlag Berlin Heidelberg, 1993.

Wittkopf, J.J.; MacDonald, M.D. 1949. Dielectric Properties of Douglas Fir at High Frequencies. Oregon State Engineering Experiment Station Bulletin 28, July 1949.

United States Department of Agriculture

Proceedings

22nd International Nondestructive Testing and Evaluation of Wood Symposium

Quebec City, Canada
2022

Photo by Gadiel Lazcano on Unsplash

Photo by Julie Boulanger on Unsplash

Photo by Gadiel Lazcano on Unsplash

Forest Service, Forest Products Laboratory
Université Laval
Forest Products Society
International Union of Forest Research Organizations

General Technical Report
FPL–GTR–290

May
2022

Abstract

The 22nd International Nondestructive Testing and Evaluation of Wood Symposium was hosted by the Université Laval in Quebec City, Canada, May 24–27, 2022. This symposium was a forum for those involved in nondestructive testing and evaluation (NDT/NDE) of wood and brought together many international researchers, NDT/NDE users, suppliers, representatives from various government agencies, and other groups to share research results, products, and technology for evaluating a wide range of wood products, including standing trees, logs, structural lumber, engineered wood products, and wood structures. Networking among participants encouraged international collaborative efforts and fostered the implementation of NDT/NDE technologies around the world. A special on-line session was conducted to accommodate individuals who could not attend in-person due to the ongoing COVID-19 pandemic. The technical content of the 22nd symposium is captured in these proceedings. Full-length, in-depth technical papers for most of the oral presentations, along with abstracts for all the oral and poster presentations, are published herein. The papers were not peer reviewed and are reproduced here as they were submitted by the authors.

Keywords: Nondestructive evaluation, nondestructive testing, wood properties, wood products, logs, trees, wood structures

May 2022

Wang, Xiping; Ross, Robert J., eds. 2022. Proceedings: 22nd International Nondestructive Testing and Evaluation of Wood Symposium. General Technical Report FPL-GTR-290. Madison, WI: U.S. Department of Agriculture, Forest Service, Forest Products Laboratory. 324 p.

A limited number of free copies of this publication are available to the public from the Forest Products Laboratory, One Gifford Pinchot Drive, Madison, WI 53726-2398. This publication is also available online at www.fpl.fs.fed.us. Laboratory publications are sent to hundreds of libraries in the United States and elsewhere.

The Forest Products Laboratory is maintained in cooperation with the University of Wisconsin.

Contents
